

Chaotic motion in the Johannsen-Psaltis spacetime

Ondřej Zelenka^{1,2,a} and Georgios Lukes-Gerakopoulos^{1,b}

¹Astronomical Institute of the Academy of Sciences of the Czech Republic,
Boční II 1401/1a, CZ-141 31 Prague, Czech Republic

²Institute of Theoretical Physics, Faculty of Mathematics and Physics,
Charles University, CZ-180 00 Prague, Czech Republic

^a ondrzel@gmail.com, ^b gglukes@gmail.com

ABSTRACT

The Johannsen-Psaltis spacetime is a perturbation of the Kerr spacetime designed to avoid pathologies like naked singularities and closed timelike curves. This spacetime depends not only on the mass and the spin of the compact object, but also on extra parameters, making the spacetime deviate from Kerr; in this work we consider only the lowest order physically meaningful extra parameter. We use numerical examples to show that geodesic motion in this spacetime can exhibit chaotic behavior. We study the corresponding phase space by using Poincaré sections and rotation numbers to show chaotic behavior, and we use Lyapunov exponents to directly estimate the sensitivity to initial conditions for chaotic orbits.

Keywords: chaos – geodesic motion – black holes

1 INTRODUCTION

We study the geodesic motion in a family of spacetimes constructed by (Johannsen and Psaltis, 2011). The corresponding metric is characterized by an infinite number of parameters, i.e. the mass M , the spin a and a series of deviation parameters ϵ_k , where $k \in \mathbb{N}_0$. However, in this work we constrain ourselves to the lowest order of the unconstrained parameters, which is ϵ_3 .

The Johannsen-Psaltis (JP) metric was designed to be a perturbation of the Kerr spacetime, which is of great astrophysical interest. The so-called *no-hair theorem* (see, e.g., Carter, 1971) states that the class of uncharged black-hole exterior solutions which are axisymmetric and don't violate causality (i.e. no closed timelike curves) consists of a discrete set of continuous families, each depending on at least one and at most two independent parameters. No other externally observable parameters are required for this description. Typically, the Kerr spacetime is assumed to describe a black hole (Rico, 2013). Kerr black holes are parametrized by their mass M and their angular momentum a . However, there is yet to be a proof if black holes are indeed described by the Kerr paradigm. Therefore,

it would be of great astrophysical interest to test this conjecture by observing black hole candidates through electromagnetic and gravitational wave signals.

The Kerr spacetime is axisymmetric and stationary, but one special feature of this spacetime is that it has an extra "hidden" symmetry that makes geodesic motion in such a background correspond to an integrable system (Carter, 1968). There are spacetimes that deviate from Kerr by a deformation parameter, these spacetimes are called in the bibliography non-Kerr spacetimes (see, e.g., Bambi, 2017). These non-Kerr spacetimes do not usually possess the symmetry that the Kerr spacetime does, making geodesic motion correspond to a non-integrable system. As a result, geodesic motion in such spacetimes exhibits chaotic behavior, which is the topic of our study.

The organization of the article is as follows: in section 2 we describe the basics of geodesic motion, deterministic chaos in dynamical systems and some of the properties of the JP spacetime. In section 3 we use numerical examples to show that the JP metric doesn't correspond to an integrable system. Section 4 summarizes our main findings. Note that geometric units are employed throughout the article, $G = c = 1$. Greek letters denote the indices corresponding to spacetime and the metric signature is $(-, +, +, +)$.

2 GEODESIC MOTION AND CHAOS

The line element of a rapidly spinning black hole introduced in (Johannsen and Psaltis, 2011) reads in Boyer-Lindquist-like coordinates

$$ds^2 = g_{tt}dt^2 + g_{rr}dr^2 + g_{\theta\theta}d\theta^2 + g_{\phi\phi}d\phi^2 + 2g_{t\phi}dtd\phi \quad , \quad (1)$$

where the metric components $g_{\mu\nu}$ (Johannsen and Psaltis, 2011) are

$$g_{tt} = -(1 + h)\left(1 - \frac{2Mr}{\Sigma}\right) \quad , \quad (2a)$$

$$g_{t\phi} = -\frac{2aMr\sin^2\theta}{\Sigma}(1 + h) \quad , \quad (2b)$$

$$g_{\phi\phi} = \frac{\Lambda\sin^2\theta}{\Sigma} + ha^2\left(1 + \frac{2Mr}{\Sigma}\right)\sin^4\theta \quad , \quad (2c)$$

$$g_{rr} = \frac{\Sigma(1 + h)}{\Delta + a^2h\sin^2\theta} \quad , \quad (2d)$$

$$g_{\theta\theta} = \Sigma \quad , \quad (2e)$$

and the metric functions are

$$\Sigma = r^2 + a^2 \cos^2 \theta , \quad (3a)$$

$$h = \sum_{k=0}^{\infty} \left(\epsilon_{2k} + \epsilon_{2k+1} \frac{Mr}{\Sigma} \right) \left(\frac{M^2}{\Sigma} \right)^k , \quad (3b)$$

$$\Delta = r^2 + a^2 - 2Mr , \quad (3c)$$

$$\omega^2 = r^2 + a^2 , \quad (3d)$$

$$\Lambda = \omega^4 - a^2 \Delta \sin^2 \theta . \quad (3e)$$

The function $h(r, \theta)$ is what causes the deviation from the Kerr metric. Namely, setting $\epsilon_k = 0 \quad \forall k \in \mathbb{N}_0$ gives the Kerr metric. The parameters $(\epsilon_k)_{k=0}^{\infty}$ are, however, constrained. As explained in detail in (Johannsen and Psaltis, 2011), we have to set $\epsilon_0 = \epsilon_1 = 0$ and the parameter ϵ_2 is constrained by observational constraints on weak-field deviations from general relativity (Johannsen and Psaltis, 2011), i.e. $|\epsilon_2| \leq 4.6 \cdot 10^{-4}$. We therefore set $\epsilon_2 = 0$ as well and limit ourselves to the lowest order remaining parameter, which is ϵ_3 , and set all the higher order parameters $\epsilon_k = 0 \quad \forall k \geq 4$.

The proper time τ defined as $d\tau^2 = -g_{\mu\nu} dx^\mu dx^\nu$ is employed as the evolution parameter. The geodesic motion of a free particle of rest mass m is then generated by the Lagrangian (see, e.g., Rindler, 2006)

$$\mathcal{L}(x^\mu, \dot{x}^\mu) = \frac{m}{2} g_{\mu\nu} \dot{x}^\mu \dot{x}^\nu , \quad (4)$$

where dot denotes a derivative with respect to the proper time. Due to the preservation of the four-velocity $g_{\mu\nu} \dot{x}^\mu \dot{x}^\nu = -1$ along a geodesic orbit $\mathcal{L} = -m/2$ is a constant. The corresponding canonical momenta are

$$p_\mu = \frac{\partial \mathcal{L}}{\partial \dot{x}^\mu} = mg_{\mu\nu} \dot{x}^\nu \quad (5)$$

and performing the Legendre transform gives the Hamiltonian

$$\mathcal{H} = \frac{1}{2m} g^{\mu\nu} p_\mu p_\nu . \quad (6)$$

The JP metric functions are independent of the parameters t and ϕ , i.e. it is stationary and axisymmetric, therefore the energy $E := -p_t$ and the component of the angular momentum $L_z := p_\phi$ are integrals of motion. This allows us to restrict our study to the meridian plane generated by the polar-like coordinates (r, θ) and move to a simpler system of two degrees of freedom. Namely, one has to merely replace

$$i = \frac{-g^{tt} E + g^{t\phi} L_z}{m}, \quad \dot{\phi} = \frac{-g^{t\phi} E + g^{\phi\phi} L_z}{m} \quad (7)$$

in the equations of motion to reduce the system. The motion in the resulting reduced system is characterized by the Newtonian-like two-dimensional effective potential

$$(p_r)^2 + \frac{g_{rr}}{g_{\theta\theta}} (p_\theta)^2 = -V_{\text{eff}} := -g_{rr} \left(1 + \frac{g_{\phi\phi} E^2 + g_{tt} L_z^2 + 2g_{t\phi} E L_z}{g_{tt} g_{\phi\phi} - g_{t\phi}^2} \right) . \quad (8)$$

For $p_\theta = p_r = 0$ the roots of this effective potential $V_{\text{eff}} = 0$ form a curve in the meridian plane, which is called the *curve of zero velocity* (CZV).

In the Kerr case, an extra "hidden symmetry" exists¹, giving rise to the Carter constant \mathcal{K} (Carter, 1968). This constant, along with E , L_z and \mathcal{H} , are independent and in involution, therefore geodesic motion in the Kerr spacetime background corresponds to an integrable system and trajectories of the reduced system lie on a family of two-dimensional *invariant tori*. These orbits oscillate in both degrees of freedom with their respective characteristic frequencies ω^r and ω^θ ; their ratio $\omega = \omega^r/\omega^\theta$ is called the *rotation number* and it is useful for the classification of orbits. If ω is rational, the torus is called *resonant* and it hosts an infinite number of periodic orbits. If ω is irrational, the motion is called *quasiperiodic* and each orbit on the torus covers it densely.

When a perturbation is applied to such an integrable system, all the resonant tori are destroyed. According to the *KAM theorem* (Meiss, 1992), however, most of the non-resonant tori survive in the perturbed system for small perturbations; these are called KAM tori. According to the *Poincaré-Birkhoff theorem* (Lichtenberg and Lieberman, 1992), where there was a resonant torus, an even number of periodic trajectories survives in the perturbed system, half of them stable and half unstable. We use a Poincaré surface of section to display the phase space structure of the system. We define a surface in the phase space and plot the intersections of the orbits with the surface. Invariant tori correspond to circles in the surface of section. These form the *main island of stability* around a stable fixed point in the center.

Near the now destroyed resonant tori, quite a different structure arises. Around the stable periodic points (corresponding to surviving stable periodic orbits), smaller islands of stability arise, forming together with the unstable points (corresponding to surviving unstable periodic orbits) *Birkhoff chains*. These unstable periodic points lie between the aforementioned islands of stability. From the unstable points emanate asymptotic manifolds, there are stable and unstable branches. The branches of the same type cannot cross each other, which results in very complicated structures in the phase space. These complicated structures are the driving engines of deterministic chaos.

An effective tool to analyze types of motion on a Poincaré section of a non-integrable system of two degrees of freedom is the angular moment v_θ , known in the literature as the rotation number (see, e.g. Voglis and Efthymiopoulos, 1998; Voglis et al., 1999). We denote the central fixed point of the main island of stability u_c and the n -th crossing of the surface of section by the orbit u_n . We define rotation angles

$$\vartheta_n := \text{ang} [u_{n+1} - u_c, u_n - u_c] \quad (9)$$

and the angular moment as

$$v_\theta = \lim_{N \rightarrow \infty} \frac{1}{2\pi N} \sum_{n=1}^N \vartheta_n \quad . \quad (10)$$

The dependence of this angular moment on the distance of the initial condition from the central fixed point is called the *rotation curve*. In an integrable system, such as the Kerr

¹ For more details on this symmetry see (Markakis, 2014) and references therein.

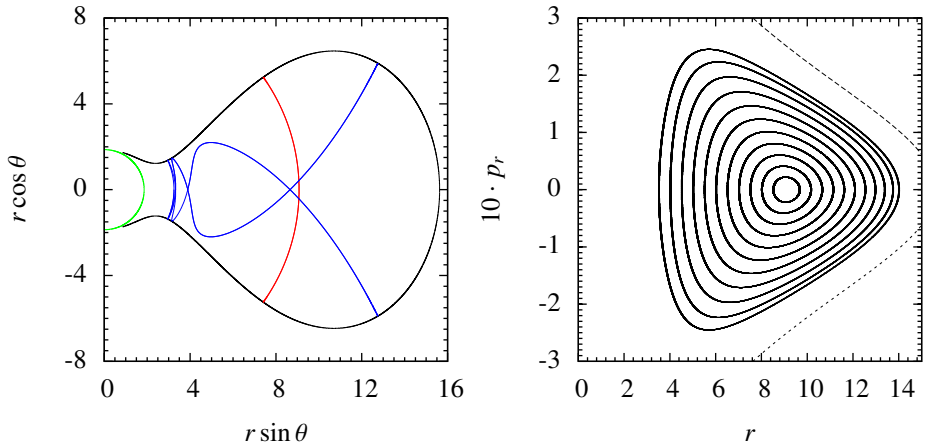


Figure 1. Left panel: projections of orbits on the meridian plane - the period-1 orbit (red), the 5/7 periodic orbit (blue), the event horizon (green), the CZV (black). Right panel: The main island of stability on the Poincaré section $\theta = \frac{\pi}{2}$.

spacetime, the rotation curve is strictly monotonous, but in a non-integrable system, it has non-monotonic variations when passing through chaotic zones, and plateaus when passing through islands of stability.

In order to quantify sensitivity to initial conditions, which is a property of chaotic systems by definition (Devaney, 1989), it is useful to define the *deviation vector* as a point of the tangent bundle of the phase space and interpret it as connecting two infinitesimally close trajectories. This vector evolves through the geodesic deviation equation

$$\ddot{\xi}^\mu + \frac{\partial \Gamma^\mu_{\kappa\lambda}}{\partial x^\nu} \dot{x}^\kappa \dot{x}^\lambda \xi^\nu + 2\Gamma^\mu_{\kappa\lambda} \dot{x}^\kappa \dot{\xi}^\lambda = 0 \quad . \quad (11)$$

As a measure of the deviation vector in a curved spacetime (see, e.g., Lukes-Gerakopoulos, 2014) we use

$$\Xi^2 := g_{\mu\nu} \xi^\mu \xi^\nu \quad . \quad (12)$$

Typically, the deviation vector follows one of two behaviors - a linear one for regular trajectories and an exponential one for chaotic trajectories. These behaviors can be detected by the *maximal Lyapunov characteristic exponent*

$$mLCE := \lim_{\tau \rightarrow \infty} \frac{1}{\tau} \log \left[\frac{\Xi(\tau)}{\Xi(0)} \right] \quad , \quad (13)$$

which gives the inverse of a characteristic deviation time scale for chaotic trajectories. In the case of regular trajectories, it behaves as $\sim \tau^{-1}$ for large τ , so in a plot in logarithmic scale it appears as a line of slope -1.

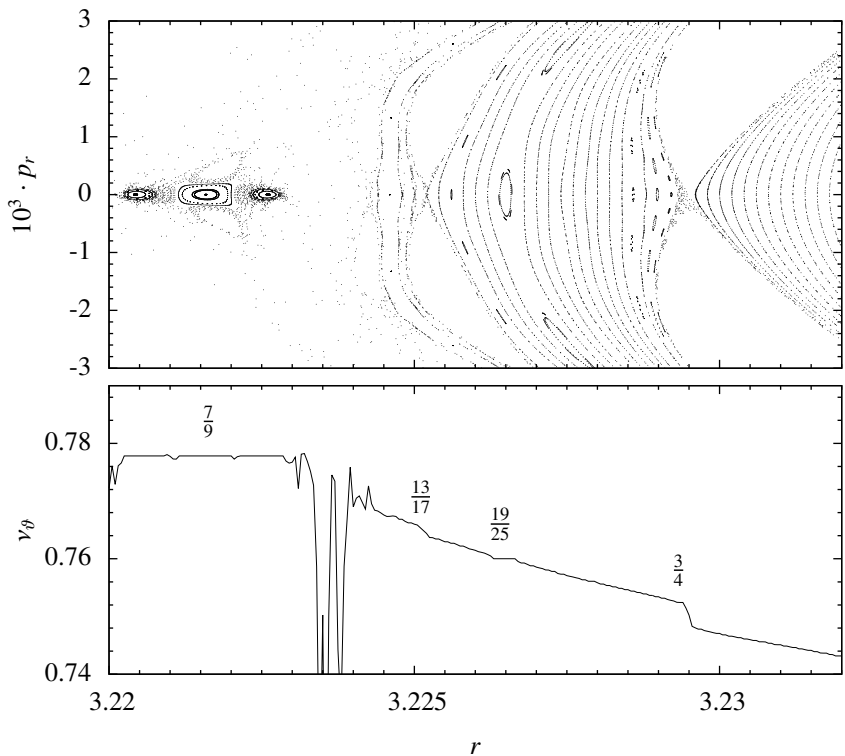


Figure 2. Top panel: Detail of the left tip of the main island of stability. Bottom panel: The rotation curve plotted for the $p_r = 0$ line of the top panel. The resonance plateaus along the curve are denoted by the respective fractions.

3 NUMERICAL EXAMPLES

All figures shown are plotted using the parameter values $M = m = 1$, $a = 0.5$, $\epsilon_3 = 0.3$, $E = 0.95$, $L_z = 2.85$. In the left panel of Fig. 1 are shown projections of two periodic orbits on the meridian plane are shown, bounded by the CZV. In the right panel, the main island of stability in the Poincaré section is shown. The equatorial plane $\theta = \pi/2$ with $\dot{\theta} > 0$ is taken as the surface of section. We notice no difference from an integrable system, as the chaotic behavior is not prominent at this broad scale depiction. This difference becomes, however, clearly visible in top panel of Fig. 2, which focuses on the left tip of the main island of stability shown in the right panel of Fig. 1. In particular, in the top panel of Fig. 2, alongside with KAM curves, appear islands of stability belonging to Birkhoff chains (ellipsoid-like structures) and chaotic zones (scattered points). Under the panel containing this detail of the surface of section, the corresponding rotation curve is plotted. The rotation curve exhibits non-monotonic variations in a chaotic zone and

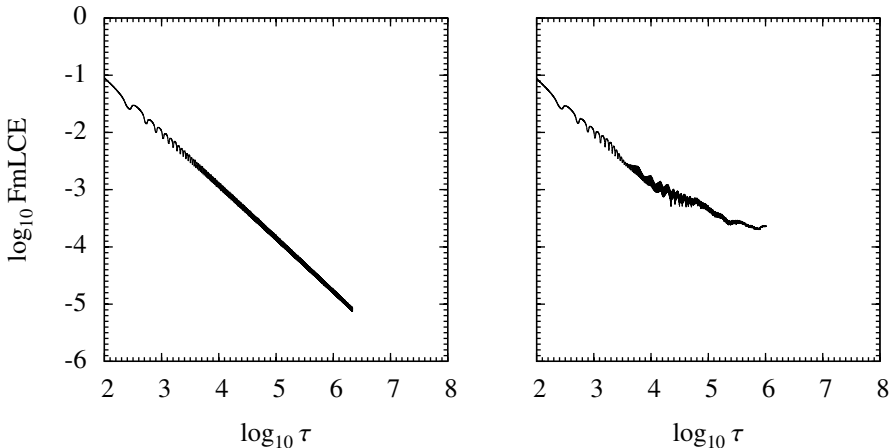


Figure 3. Convergence of mLCE for a regular orbit (left panel) with a chaotic orbit (right panel). Both orbits starting with $p_r = 0$ on the surface of section shown in Fig. 2, the regular from $r = 3.226$ and the chaotic from $r = 3.2294$.

plateaus (denoted by the corresponding fraction) along islands of stability. Thus, Fig. 2 indicates that the JP spacetime corresponds to a non-integrable system.

To directly estimate the sensitivity to initial conditions, we have calculated the mLCE. Fig. 3 shows the convergence of the mLCE for one regular (left panel) and one chaotic orbit (right panel). For the regular orbit indeed the mLCE convergence follows the -1 slope, while for the chaotic orbit the mLCE converges to a positive value.

4 CONCLUSION

We have shown by numerical examples that geodesic motion in the JP spacetime background corresponds to a non-integrable system, since chaos was detected. The astrophysical implication is that if the spacetime around black holes is not described by the Kerr metric, then one should expect imprints of chaos in electromagnetic and gravitational wave signals coming from systems like extreme mass ratio inspirals.

ACKNOWLEDGEMENTS

O.Z. and G.L-G are supported by Grant No. GACR-17-06962Y of the Czech Science Foundation. We thank Petra Suková and Ondřej Kopáček for useful discussions.

REFERENCES

- Bambi, C. (2017), *Black holes : a laboratory for testing strong gravity*, Springer, Singapore, ISBN 978-981-10-4524-0.
- Carter, B. (1968), Global structure of the kerr family of gravitational fields, *Phys. Rev.*, **174**, pp. 1559–1571, URL <https://link.aps.org/doi/10.1103/PhysRev.174.1559>.
- Carter, B. (1971), Axisymmetric black hole has only two degrees of freedom, *Phys. Rev. Lett.*, **26**, pp. 331–333, URL <https://link.aps.org/doi/10.1103/PhysRevLett.26.331>.
- Devaney, R. (1989), *An Introduction to Chaotic Dynamical Systems*, Addison-Wesley advanced book program, Addison-Wesley, ISBN 9780201130461, URL <https://books.google.cz/books?id=e1PvAAAAMAAJ>.
- Johannsen, T. and Psaltis, D. (2011), Metric for rapidly spinning black holes suitable for strong-field tests of the no-hair theorem, *Phys. Rev. D*, **83**, p. 124015, URL <https://link.aps.org/doi/10.1103/PhysRevD.83.124015>.
- Lichtenberg, A. and Lieberman, M. (1992), *Regular and Chaotic Dynamics*, Second Edition, Springer-Verlag, New York, ISBN 0-387-97745-7.
- Lukes-Gerakopoulos, G. (2014), Adjusting chaotic indicators to curved spacetimes, *Phys. Rev. D*, **89**, p. 043002, URL <https://link.aps.org/doi/10.1103/PhysRevD.89.043002>.
- Markakis, C. (2014), Constants of motion in stationary axisymmetric gravitational fields, *Monthly Notices of the Royal Astronomical Society*, **441**, pp. 2974–2985, arXiv: [1202.5228](https://arxiv.org/abs/1202.5228).
- Meiss, J. D. (1992), Symplectic maps, variational principles, and transport, *Rev. Mod. Phys.*, **64**, pp. 795–848, URL <https://link.aps.org/doi/10.1103/RevModPhys.64.795>.
- Rico, J. M. A. (2013), *The Kerr black hole hypothesis: a review of methods and results*, Master's thesis, Lisbon, CENTRA, URL <https://fenix.tecnico.ulisboa.pt/downloadFile/395145712687/dissertacao.pdf>.
- Rindler, W. (2006), *Relativity: special, general, and cosmological*, Oxford Univ. Press, 2 edition.
- Voglis, N., Contopoulos, G. and Efthymiopoulos, C. (1999), Detection of ordered and chaotic motion using the dynamical spectra, *Celestial Mechanics and Dynamical Astronomy*, **73**(1), pp. 211–220, ISSN 1572-9478, URL <http://dx.doi.org/10.1023/A:1008307332442>.
- Voglis, N. and Efthymiopoulos, C. (1998), Angular dynamical spectra. a new method for determining frequencies, weak chaos and cantori, *Journal of Physics A: Mathematical and General*, **31**(12), p. 2913, URL <http://stacks.iop.org/0305-4470/31/i=12/a=015>.